Pulmonary Surfactant Protein A-Mediated Enrichment of Surface-Decorated Polymeric Nanoparticles in Alveolar Macrophages

Christian A. Ruge,[†] Hervé Hillaireau,[†] Nadège Grabowski,[†] Mortiz Beck-Broichsitter,[†] Olga Cañadas,[‡,§] Nicolas Tsapis,[†] Cristina Casals,[‡,§] Julien Nicolas,[†] and Elias Fattal*,[†]

[†]Institut Galien Paris-Sud, Univ. Paris-Sud, CNRS, Université Paris-Saclay, 92296 Châtenay-Malabry, France
[‡]Department of Biochemistry and Molecular Biology I, Universidad Complutense, 28040 Madrid, Spain
[§]CIBER de Enfermedades Respiratorias, Universidad Complutense, 28040 Madrid, Spain

S *Supporting Information*

ABSTRACT: Surfactant protein A (SP-A), a lung anti-infective protein, is a lectin with affinity for sugars found on fungal and micrococcal surfaces such as mannose. We synthesized a mannosylated poly(lactic acid)−poly(ethylene glycol) (PLA−PEG) copolymer and used it to produce nanoparticles with a polyester (PLGA/PLA) core and a PEG shell decorated with mannose residues, designed to be strongly associated with SP-A for an increased uptake by alveolar macrophages. Nanoparticles made of the copolymers were obtained by nanoprecipitation and displayed a size of around 140 nm. The presence of mannose on the surface was demonstrated by zeta potential changes according to pH and by a strong aggregation in the presence of concanavalin A. Mannosylated nanoparticles bound to SP-A as demonstrated by dynamic light scattering and transmission electron microscopy. The association with SP-A increased nanoparticle uptake by THP-1 macrophages in vitro. In vivo experiments demonstrated that after intratracheal administration of nanoparticles with or without SP-A, SP-A-coated mannosylated nanoparticles were internalized by alveolar macrophages in greater proportion than SP-A-coated nonmannosylated nanoparticles. The data demonstrate for the first time that the pool of nanoparticles available to lung cells can be changed after surface modification, using a biomimetic approach.

KEYWORDS: *surfactant protein A, mannose, nanoparticles, macrophages, lungs*
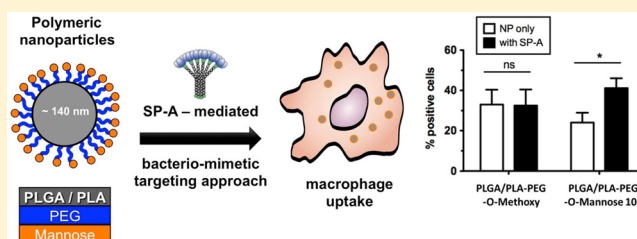
INTRODUCTION

Lung delivery of drug-loaded nanoparticles (NPs) represents an interesting strategy for the treatment of pulmonary infectious or inflammatory diseases.[1] However, in the design of advanced drug delivery systems, targeting strategies allowing for spatially controlled drug release and action are of increasing importance. Drug targeting to the lungs can be considered as controlled delivery to a defined region of the respiratory tract, controlled delivery to the site of disease (e.g., tumor tissue), or controlled delivery to specific cells (e.g., infected macrophages).[2] Principally, by focusing the drug action to the cellular site of disease, it is possible to overall reduce the dose needed to obtain the desired therapeutic effect and to consequently reduce the extent of unwanted side effects.[2,3] This overall leads to more selective treatments.

In that respect, polymer-based NPs designed as drug carrier are of special interest since it is possible to chemically control their molecular composition with a great variety of ligands. Indeed, the "polymer−chemical toolbox" holds sheer endless opportunities to design and synthesize materials with defined properties that allow for the preparation of NPs that are colloidally stable, biocompatible, and biodegradable according to the requirements of their medical applications.

The most interesting aspect in the design of such novel materials is probably the chemical coupling of targeting ligands to polymers. On the one hand, a targeting ligand may enhance the selective binding to subcellular structures of distinct cell types (e.g., surface receptors) and increase hereby the extent by which the modified NPs interact with targeted cells. On the other hand, a targeting ligand may additionally trigger a subsequent biological action such as receptor-mediated uptake into cells. In this respect, a common approach is to functionalize the polymer or NP with ligands whose receptors are overexpressed on the cell type to be targeted.[4] Among the polymers used to design such systems, poly(lactide-*co*-glycolide) (PLGA) copolymers were recently shown to be quite safe toward macrophages and lung cells[5−7] and *in vivo* after lung instillation.[8] One strategy to target specific cells such as lung macrophages would be to design biomimetic nanoparticulate systems with a surface decorated by a relevant protein recognized by macrophages. One such relevant

candidate is pulmonary surfactant protein A (SP-A), the most abundant protein associated with lung surfactant.[9]

Pulmonary surfactant is a complex surface-active lipo-protein matrix located at the air−liquid interface that prevents the alveoli of the lungs from collapsing. Thus, it is naturally required for proper lung function.[10] SP-A has four regions: (i) a globular carbohydrate recognition domain (CRD), (ii) a neck-region, (iii) a collagenous stem domain, and (iv) a N-terminal region. While the collagenous stem is mostly responsible for interactions with cellular surface receptors, the CRD is relevant for recognition of carbohydrate motives present on bacterial or viral surfaces and thus opsonizing such structures.[11] It is known that, among relevant carbohydrates, SP-A has affinity for mannose and fructose.[9] The inevitable interaction with SP-A and opsonization leads to enhanced recognition by cells of the host defense system, such as alveolar macrophages (AM), and triggers an immune response that results in an overall more efficient removal of pathogens or particulates from the lungs.[12,13]

However, some pathogens exploit this interaction in order to invade host cells as a biological niche. For instance, it is known that both SP-A and surfactant protein receptors play an important role in the invasion of *Mycobacterium tuberculosis* (Mtb) in AM after it enters the human body via inhalation.[14,15] Upon pulmonary deposition, Mtb parasitizes AM and resides inside these professional phagocytes.[16] Since it is very difficult to efficiently treat Mtb infection,[17] an interesting approach would be to design a system that mimics Mtb and follows the pathway by which the pathogen is internalized in order to end in close intracellular proximity to the bacteria.[18] However, such a carrier system would be required to be in a size range below approximately 200 nm to avoid nonspecific phagocytosis and should be covered with SP-A for receptor mediated internalization.

In this article, we have designed such NPs that specifically interact with the CRD of SP-A in order to enhance their uptake by AM. Following a biomimetic approach by imitating Mtb's pathway of cell entering, we demonstrate it is possible to target efficiently macrophages *in vitro* and in AM *in vivo*.

■ EXPERIMENTAL SECTION

General. All reagents were used without further purification. D,L-Lactic acid was purchased from Biovalley, Polysciences Inc. (Germany). α-Diethyl-acetal-propionaldehyde-terminated-poly-(ethylene glycol) (HO-PEG-Acetal; M_n = 3600 g·mol^{-1}) was purchased from Polymer Source (Canada). Tin(II)-2-ethyl-hexanoate (stannous octoate, 95%), 4-aminophenyl-α-D-mannopyranoside, and sodium cyanoborohydride were purchased from Sigma−Aldrich (France). Poly(D,L-lactide-*co*-glycolide) (PLGA, Resomer RG756) was obtained from Boehringer Ingelheim (Germany). The Rhodamine-B−PLGA conjugate (AV11; M_n ≈ 30000 g·mol^{-1}) was acquired from Akina Inc. (USA). Synthetic 1,2-dipalmitoyl-*sn*-glycero-3-phosphocholine (DPPC; 16:0/16:0) was received from Corden Pharma (Germany). 1-Palmitoyl-2-oleoyl-*sn*-glycero-3-phospho-rac-glycerol (POPG) was purchased from Avanti Polar Lipids (USA). Palmitic acid (PA) was obtained from Sigma-Aldrich. All other reagents were purchased from Sigma-Aldrich unless not otherwise stated. All solvents used were of analytical grade.

Synthesis of PLA-*b*-PEG-acetal. α-Diethyl-acetal-propionaldehyde-terminated poly(lactide)-*block*-poly(ethylene glycol) (PLA-*b*-PEG-acetal) was synthesized by ring opening polymerization of lactic acid from a hydroxyl-end-functionalized-poly(ethylene glycol) macroinitiator in the presence of a stannous octoate catalyst.[19,20] Briefly, lactic acid (1.5 g, 10.4 mmol), HO-PEG-acetal (0.08 g, 0.022 mmol), and stannous octoate (0.01 g, 0.025 mmol; 1.14 mol/mol PEG) dissolved into 2 mL of dried toluene (Sigma-Aldrich) were added to a 10 mL Schlenk tube (flame-dried and cooled under a flow of dry argon). Polymerization was carried out for 100 min in an oil bath at 130 °C with continuous stirring under a gentle, continuous flow of argon. The reaction was stopped by immersion of the tube into an ice−water bath. After evaporation of toluene using a Rotavap (Büchi, Switzerland), the product was dissolved in a minimal amount of chloroform and precipitated into cold diethyl ether to remove stannous octoate and unreacted lactide. The obtained product was then dissolved in tetrahydrofuran (THF) and precipitated into water in order to remove unreacted PEG. The final copolymer was lyophilized (Christ Alpha 1−2 LD plus, Germany) and stored at −20 °C until usage.
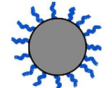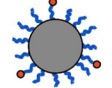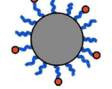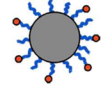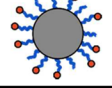
A PLA-*b*-PEG-methoxy copolymer was also synthesized following the same protocol after respective adjustment of the reaction conditions (40 min at 120 °C), while an α-hydroxy-ω-methoxy-poly(ethylene glycol) macroinitiator (0.022 mmol, M_n = 5000 g·mol^{-1}; Sigma-Aldrich) and 0.015 mmol stannous octoate were used instead.

Synthesis of PLA-*b*-PEG-mannose. Mannosylated PLA-*b*-PEG (PLA-*b*-PEG-mannose) was synthesized according to a modified protocol published by Jule et al.[21] Briefly, PLA-*b*-PEG-acetal was dissolved in *N*,*N*-dimethylacetamide (DMAc) at a concentration of 5 mg·mL^{-1} and subsequently filtered through a PFTE filter unit (0.45 μm pore size; VWR International, Germany) into a preswollen regenerated cellulose dialysis membrane (MWCO 3500 Da; SpectrumLabs, France). The solution was dialyzed for 24 h against a 100-fold excess of Milli-Q water (Millipore Corporation, USA) with exchange of water after 2, 5, and 8 h. Subsequently, the obtained colloidal solution was adjusted to a concentration of ∼1.5 mg·mL^{-1}, and the PEG-terminal acetal functions were deprotected by adjustment of the solution to pH 2 under stirring (300 rpm) using 0.1 M HCl. After 2 h of stirring, the pH of the solution was adjusted to pH 7 using 0.1 M NaOH, and a small volume was taken for evaluation of the aldehyde functionality. Then, the solution was concentrated to ∼3−4 mg·mL^{-1} using a Rotavap (Büchi, Switzerland) before introducing a 15-fold molar excess of 4-aminophenyl-α-D-mannopyranoside (31 μmol, 8.48 mg). The solution was stirred for 1.5 h, followed by reduction of the resulting Schiff base to a secondary aromatic amine using a 15-fold molar excess of NaH$_3$BCN (31 μmol, 2 mg). After additional stirring for 96 h, the product was dialyzed using a preswollen membrane (SpectrumLabs, MWCO 3500 Da) for 24 h (water exchange after 2, 5, and 8 h). The copolymer was once more lyophilized and stored at −20 °C until use.

Characterization of PLA-*b*-PEG. ^{1}H NMR spectroscopy of PLA-*b*-PEG was performed in NMR tubes (∅ 5 mm) in DMSO-d_6 (VWR) on a Bruker Avance-300 (400 MHz) spectrometer and was used to determine the number-average molecular weight (M_n) of the PLA-*b*-PEG copolymer.

Size exclusion chromatography (SEC) was performed on a Malvern Instruments triple-detector SEC setup (GPCmax) composed of an online degasser, a pump, an automatic sampler, one precolumn (10 × 4.6 mm, bead diameter 8 μm), and two columns (T4000, 300 × 7.8 mm, bead diameter 7 μm, exclusion limit 4 × 10^5 g·mol^{-1}, pore size 1500 Å; and T3000,

Table 1. Physico-Chemical Characterization of Mannosylated Nanoparticle Formulations

Nanoparticle type	Nanoparticle formulation name	PLA-*b*-PEG-mannose/ PLA-*b*-PEG w/w ratio	Fraction of mannose residues on nanoparticle surface (%) [#]	Average hydro-dynamic diameter (nm) [##]	Poly-dispersity index (PdI) [##]	Zeta potential (mV) [##]
	PLGA/PLA@PEG	0 : 100	0	144 ± 7	0.096 ± 0.045	−26.8 ± 2.0
	PLGA/PLA@PEG @mannose (25)	25 : 75	16	140 ± 6	0.114 ± 0.035	−30.6 ± 4.9
	PLGA/PLA@PEG @mannose (50)	50 : 50	32	138 ± 9	0.122 ± 0.007	−30.3 ± 4.2
	PLGA/PLA@PEG @mannose (75)	75 : 25	48	139 ± 5	0.124 ± 0.008	−28.8 ± 2.9
	PLGA/PLA@PEG @mannose (100)	100 : 0	65	146 ± 10	0.114 ± 0.018	−29.0 ± 1.7

[#]Fraction of mannose residues present on PEG chain extremities, based on integration of the NMR signals of *p*-aminophenyl-mannopyranoside groups and acetal end groups at 6.5 and 7.0 ppm, respectively. [##]Measurements performed in 1 mM NaCl at pH ≈ 7, data shown as mean ± SD ($n \geq 4$).

300 × 7.8 mm, bead diameter 6 μm, exclusion limit 7 × 10^4 g·mol^{-1}, pore size 500 Å) from Malvern Instruments, and a triple detector array (TDA) including in series RALLS (right-angle laser light scattering), LALLS (low-angle laser light scattering) at 7°, refractometer, and finally viscometer. The software (OmniSEC) corrects for interdetector delay and makes partial correction for band broadening. The eluent was DMAc with 0.5% lithium bromide at 50 °C and at a flow rate of 0.7 mL·min^{-1}.

Preparation of Mannosylated Nanoparticles. NPs were prepared using the solvent displacement technique according to a modified protocol published elsewhere.[22] Briefly, 4 mg of a physical mixture of PLA-*b*-PEG and PLA-*b*-PEG-mannose copolymers (100:0, 25:75, 50:50, 75:25, or 0:100 w/w) was dissolved in 2 mL of a PLGA solution in THF (3.5 mg·mL^{-1} PLGA, containing 5% (w/w) Rhodamine-B−PLGA). This organic solution was constantly injected into a magnetically stirred aqueous phase (6 mL, 800 rpm) using a 2.5 mL glass syringe (Hamilton, Switzerland), equipped with a 0.6 × 25 mm injection needle (Terumo Medical Corp., USA). The resulting colloidal suspension was continuously stirred under a fume hood until complete evaporation of the organic solvent. Finally, the obtained NP formulation, respectively, was passed through a Millex-AP filter (2 μm pore size; Millipore) in order to remove potential dust contaminations. The NP size distribution was not affected by this filtration step. Nanoparticle types and names are summarized in Table 1.

Size, Zeta Potential, and Transmission Electron Microscopy Observation of Nanoparticles. The hydro-dynamic diameter (Z-average) and polydispersity index (PdI) of the prepared NPs were measured by dynamic light scattering using a Zetasizer Nano ZS instrument (Malvern, France). Samples were diluted in 1 mM NaCl to a final concentration of about 100 μg·mL^{-1}. In order to assess stability of the formulations in cell culture relevant conditions, NPs diluted

in cell culture medium (100 μg·mL^{-1}) (see cell culture section for medium composition) were incubated at 37 °C in a humidified 5% CO$_2$ atmosphere for 4 h. Measurements were performed at 25 °C and at an angle of 173°. The measurement duration was set at 60 s. The zeta potential (ζ) was measured with the same instrument at 25 °C using a folded capillary cell. Measurements were carried out in 1 mM NaCl or in 5 mM HEPES buffer (Sigma−Aldrich) at pH 2−7 (conductivity adjusted to ∼1−2 mS·cm^{-1}). Measurements were performed in triplicate.

Transmission electron microscopy (TEM) was performed using a JEOL JEM-1400 microscope operating at 80 kV. The respective NP suspensions (∼1 mg·mL^{-1}) were deposited onto copper grids (400 mesh) covered with a Formvar film for 1 min. In order to enhance the contrast, a negative staining (30 s) with 1% phosphotungstic acid was performed. The excess solution was removed using filter paper, and the grids were air-dried before microscopic analysis. Image acquisition was performed using a high-resolution camera, Advantage HR3/12GO4 (AMT-Hamamatsu).

Isolation of Surfactant Protein A. Human surfactant protein A was isolated from bronchoalveolar lavage (BAL) of patients with alveolar proteinosis using a sequential butanol and octylglucoside extraction.[23−25] The purity of SP-A was checked by one-dimensional SDS-PAGE in 12% acrylamide under reducing conditions and mass spectrometry. The oligomerization state of SP-A was assessed by electrophoresis under nondenaturing conditions,[24,25] electron microscopy,[25] and analytical ultracentrifugation as reported elsewhere.[24] SP-A consisted of supratrimeric oligomers of at least 18 subunits (MW, 650 kDa). The biological activity of isolated SP-A was assayed by testing its ability to self-associate in the presence of calcium at 37 °C[23] and to induce phospholipid vesicle and bacterial lipopolysaccharide aggregation.[24,25]

Concanavalin-A Agglutination Assay. The presence of mannose residues on the NP surface was assessed in a concanavalin A (ConA) agglutination assay. Briefly, NP formulations were diluted in ConA assay buffer (5 mM HEPES, 150 mM NaCl, 1 mM $CaCl_2$, 1 mM $MnCl_2$, pH 6.5) to a final concentration of 100 $\mu g \cdot mL^{-1}$. After 5 min size measurement at 25 °C (Zetasizer Nano ZS), 80 μL of ConA aqueous solution was added to the NP suspensions (2 μM final ConA concentration), and the particle size was measured for another 15 min.

Nanoparticle−SP-A Interaction. The interaction between NPs and SP-A was first assessed by size measurement. Briefly, NPs were dispersed at 200 $\mu g \cdot mL^{-1}$ in Tris-HCl buffer (5 mM Tris, 150 mM NaCl, 1 mM $CaCl_2$, pH 7.4) and measured in a quartz glass cuvette at 25 °C with a measurement of 60 s. After 5 min, the measurement was interrupted for addition of SP-A at a final concentration of 20 $\mu g \cdot mL^{-1}$, and the sample was measured for another 15 min.

For TEM analysis of NP−SP-A complexes, NP formulations were dispersed at 200 $\mu g \cdot mL^{-1}$ in Tris-HCl buffer, and SP-A was added at a final concentration of 20 $\mu g \cdot mL^{-1}$. The samples were incubated for 30 min at RT and afterward kept on ice until analysis. Deposition of the samples onto copper grids was performed without further dilution. Staining of samples was carried out using a 30 s incubation with 1% phosphotungstic acid.

Preparation of Surfactant Lipid Vesicles. Lipid vesicles were prepared as described elsewhere.[26,27] Briefly, a lipid stock solution (20 $mg \cdot mL^{-1}$) in chloroform/methanol (2:1, v/v) was prepared for DPPC, POPG, and PA, respectively. Appropriate volumes of each stock solution were mixed to obtain a final weight ratio of 28:9:5.6 (DPPC/POPG/PA) with a total lipid mass of 1 mg. The organic solvents were evaporated under nitrogen with subsequent centrifugation under reduced pressure for 1 h using a vacuum centrifuge (Eppendorf Concentrator 5301, Eppendorf Germany). The dried lipid mixture was rehydrated with 1 mL of PBS by placing the sample in a water bath (50 °C) with alternating subsequent vortexing. The resulting multilamellar suspension was sonicated for 3 min (bursts of 0.6 s with 0.4 s between bursts) using a 2 mm microtip with a Branson Digital Sonifier 250 (Danbury, CT, USA) at 10% amplitude to obtain unilamellar vesicles.

Cell Culture. The THP-1 cell line was obtained from ATCC (catalog number TIB-202) and cultured in RPMI-1640 growth medium (Sigma), supplemented with 50 $U \cdot mL^{-1}$ penicillin, 50 $U \cdot mL^{-1}$ streptomycin, and 10% (v/v) fetal calf serum (FCS; Lonza, Belgium). Cells were maintained at 37 °C in a 5% CO_2 humidified atmosphere and used from passage 3 to 15 after thawing. Cytotoxicity and uptake experiments were performed using monocyte-derived macrophages, obtained from THP-1 cells incubated for 48 h with 10 nM 12-O-tetradecanoylphorbol-13-acetate (PMA; Sigma-Aldrich). Such conditions have been previously shown to induce differentiation of THP-1 monocytes into functional CD11b$^+$, CD14$^+$ macrophages.[28]

Nanoparticle Uptake Experiments. *Flow Cytometry.* NP uptake with or without SP-A and surfactant lipids was studied in THP-1 derived macrophages. Briefly, cells were seeded in 1 mL of growth medium (3 × 10^5 cells·mL^{-1}; 10 nM PMA) in 24-well plates (TTP) and cultured for 48 h. After medium renewal and 24 h incubation, 300 μL of NP formulations (final concentration 50 $\mu g \cdot mL^{-1}$, NPs containing 5% (w/w) Rhodamine-B−PLGA) dispersed in RPMI-1640 (0.5% FCS)

were added to the cells and incubated for 0.5, 1, 2, or 3 h, respectively. In order to study the effect of SP-A (with and without surfactant lipids), NPs dispersed in RPMI-1640 (0.5% FCS) containing 5 to 20 $\mu g \cdot mL^{-1}$ SP-A (supplemented with or without 25 to 100 $\mu g \cdot mL^{-1}$ surfactant lipids) were added to the cells and incubated for 3 h. After incubation, supernatants were discarded and cells were rinsed twice with warm PBS before harvest by trypsinization. Cell suspensions were analyzed by flow cytometry (BD Accuri C6; Becton Dickinson, USA), and the mean fluorescence intensities (MFI) of 5000−10000 gated events were collected at 585/40 nm. Results were expressed as percentage of cells with higher MFI compared to untreated cells (% positive cells).

Confocal Microscopy. Cells were seeded in 300 μL of growth medium (1.5 × 10^6 cells·mL^{-1}; 10 nM PMA) on 8-well chamber slides (Labtek I; Thermo Scientific, France) and cultured for 48 h. Uptake experiments were performed as described above for flow cytometry. After 3 h incubation of the NPs in the absence or presence of SP-A (10 $\mu g \cdot mL^{-1}$), supernatants were discarded and cells were rinsed twice with warm PBS before fixation with 4% paraformaldehyde (4 °C, 10 min). After one final washing step with PBS, the uptake of NPs (containing 5% (w/w) Rhodamine-B−PLGA) into cells was observed with a LSM510 Meta confocal microscope (Zeiss, Germany), equipped with argon (488 nm, 300 mW) and helium−neon (543 nm, 5 mW) lasers, and a plan-apochromat 63× objective (numerical aperture 1.40, oil immersion). Red fluorescence was collected with a long-pass 560 nm emission filter under a 543 nm excitation wavelength. Images were processed with Volocity software (Version 5.0).

Animals. Balb/cJcR female mice were purchased from Janvier Laboratories. Food and water were administered ad libitum. Mice were housed in plastic cages under controlled environmental conditions (temperature 19−21 °C, humidity 40−70%, light during 12 h per day). Mice were acclimated to these conditions for 7 days before experiments started. The rules from the local ethics committee (protocol number 2012−117) were followed.

Pulmonary Administration of Nanoparticles. Mice (6 week old, ~17 g) were randomly divided into groups of n = 5−6. Intratracheal aerosol application was performed according to the protocol previously described.[8] Briefly, mice were anesthetized using a combination of 47 $g \cdot kg^{-1}$ ketamine and 1.2 $g \cdot kg^{-1}$ xylazine. About 10 to 15 min after intraperitoneal injection, mice were exposed to isoflurane 3% up to the loss of the pedal reflex. For intratracheal aerosol application of NPs, mice were suspended in supine position by the upper teeth at a 45° angle on an intubation platform (Hallowell EMC, USA). The mouth was opened, and the tongue was displaced with the help of forceps. Then, a mouse laryngoscope (LS-2, Penn-century Inc., USA) was inserted for oropharyngeal visualization. Once a clear view of the trachea was obtained (visualization of the vocal chords), the tip of a MicroSpray Aerosolizer (MicroSprayer model IA-1C, equipped with a FMJ-250 High Pressure Syringe, Penn-century Inc., USA) was endotracheally introduced until the carina was reached, and 50 μL of NP suspension, in native state or preincubated with SP-A as described above, or PBS (control) were instilled. The tip was withdrawn, and the mouse was removed from the support and allowed to recover for a period of 15−25 min before being placed back in cage.

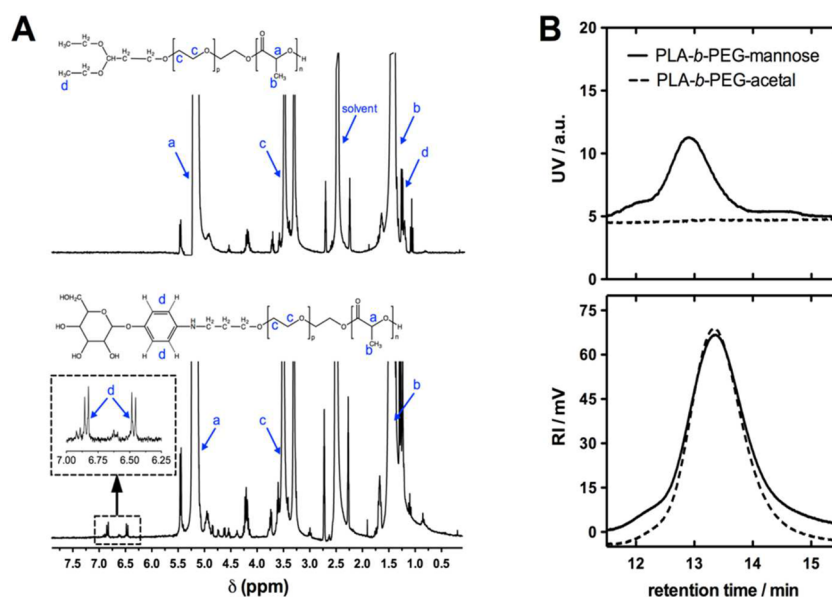**Nanoparticle Uptake by Pulmonary Macrophages.** After 4 h, mice were euthanized using a lethal dose of

Figure 1. Synthesis of PLA-*b*-PEG-mannose. (A) ^{1}H NMR (300 MHz) spectra (8−0 ppm region in d_6-DMSO) of purified PLA-*b*-PEG (acetal form) (top) and PLA-*b*-PEG-mannose (bottom). (B) Size exclusion chromatograms (UV and refractive index detection, respectively) of PLA-*b*-PEG before (acetal form) and after conversion with *p*-aminophenyl-mannopyranoside (PLA-*b*-PEG-mannose).

pentobarbital, and the bronchoalveolar lavage (BAL) was immediately performed as described elsewhere.[29,30] Briefly, the trachea was surgically exposed and a small incision was made between tracheal rings to allow the insertion of a polyethylene tube attached to a short 21G syringe needle. Lungs were instilled successively with isotonic ice-cold saline that was gently retrieved. Five lavages of 700 μL were performed and pooled. One milliliter of BAL (∼100000 cells) was centrifuged (1400 rpm, 4 min) and resuspended in 90 μL of PBS (1% (w/v) BSA). After blocking of unspecific Fc-receptors by incubation with purified Rat Anti-Mouse CD16/CD32 (Catalog No. 553142, BD Biosciences, France) at 1:100 in PBS (1% BSA) for 15 min at 4 °C, the cells were washed once with PBS (1% BSA) and subsequently stained with anti-CD11c (APC Hamster Anti-Mouse CD11c, Catalog No. 561119, BD Biosciences, France) at 1:200 in PBS (1% BSA) for 30 min at 4 °C. After one final washing step with PBS (1% BSA), cells were subjected to flow cytometric analysis applying a gating strategy described by Vermaelen et al.[31] Nanoparticle uptake was assessed based on the rhodamine fluorescence measured in the gate corresponding to AM.

Statistical Analysis. Statistical analysis was carried out in GraphPad Prism 5.0 (GraphPad Software Inc., USA) using one-way ANOVA followed by Newman−Keuls posthoc tests. Statistical differences between groups in Figure 6 were determined by *t*-test. For all tests $p < 0.05$ was considered as significant difference.

■ RESULTS AND DISCUSSION

Polymer Synthesis and Characterization. The main goal of this study was to design a polymer building block for the formulation of NPs that can specifically interact with SP-A as a targeting ligand associated with NPs via mannose residues. It was recently shown that SP-A can enhance the NP uptake in AM.[26,32] However, the particles used in those studies had model characteristics and were not biodegradable and thus less suited for drug delivery purposes. Furthermore, there was a lack of specificity regarding the interaction between SP-A and the

NP surface since the enhanced binding of SP-A was due to an overall affinity of the protein to lipophilic patterns.[26] This is the reason why NPs made of the biodegradable (co)polymers PLA and PLGA were designed in this study, which offers diverse opportunities for polymer functionalization with moieties for enhanced stability and/or target structure recognition.[33] In the case of small molecule ligands, functionalization is commonly performed directly on the polymer dissolved in homogeneous media (typically in organic solvents) prior to NP formulation, while large biomolecular ligands (such as peptides, proteins, or antibodies) are usually immobilized on the already prepared NPs.[33] Here, we successfully synthesized a PLA-*b*-PEG copolymer that allows for selective functionalization with a mannose residue without changing the copolymer dispersity. Polymer synthesis was carried out following a two-step approach. In the first step, we applied ring opening polymerization (ROP) to synthesize a poly(lactide)-*block*-poly(ethylene glycol) copolymer (PLA-*b*-PEG) following the protocol recently described by Diou et al.,[19] using a 3 kDa of α-diethyl-acetal-propionaldehyde-terminated-poly(ethylene glycol) (OH-PEG-acetal) as macromolecular initiator. In the second step, the terminal acetal-group of the intermediate PLA-*b*-PEG copolymer was deprotected and the free aldehyde was converted with an aminophenyl-mannopyranoside component in order to form a Schiff base, which was then reduced to obtain the final product PLA-*b*-PEG-mannose. The chemical composition, molecular weight, and coupling yield of the functionalized copolymer PLA-*b*-PEG-mannose was determined from ^{1}H NMR spectra (Figure 1A). The reaction conditions were optimized to obtain a PLA-*b*-PEG-acetal with a molecular weight of 45 kDa as determined from ^{1}H NMR spectroscopy, in order to obtain a sufficiently long PLA chain allowing for NPs preparation (Supporting Information, Figure S1). NMR spectra of PLA-*b*-PEG-acetal showed specific signals for the diethyl-groups (see 'd' in top spectrum in Figure 1A). These signals disappeared after deprotection of the acetal-group under acidic conditions, while instead a NMR signal at ∼9 ppm could be detected, which corresponded to the free aldehyde (data not

shown). After conversion of the free aldehyde with *p*-aminophenyl-mannopyranoside and reduction of the Schiff base, PLA-*b*-PEG-mannose was obtained. The signals corresponding to the phenyl protons (6−7 ppm) were integrated to determine the degree of functionalization of the final copolymer (see inset in bottom spectrum in Figure 1A), which was found to be between 60 and 65%. Additionally, the obtained copolymers were analyzed by size exclusion chromatography (SEC). Comparison of chromatograms from refractive index (RI) detection showed a homogeneous size distribution of the copolymers, indicating no significant changes to the copolymer after its chemical modification with mannose (see bottom chromatogram in Figure 1B). SEC in combination with UV-detection revealed an increase on the UV-signal in the case of PLA-*b*-PEG-mannose, verifying the presence of an UV-active phenyl-group homogeneously attached to the PLA-*b*-PEG copolymer (see top chromatogram in Figure 1B).

Nanoparticle Preparation and Characterization. Using the obtained amphiphilic PLA-*b*-PEG and PLA-*b*-PEG-mannose copolymers, the NPs were obtained by the nanoprecipitation method.[22] The undeniable advantages of this method are its scalability and the feasibility to prepare NPs without stabilizers, which otherwise could interfere with the SP-A binding or cellular recognition. NP preparation was investigated in combination with PLGA, in order to obtain NPs with a hydrophobic core (PLGA and PLA segment of the copolymers) and a hydrophilic shell (PEG segments) decorated with mannose (PLGA/PLA@PEG@mannose). Systematic optimization following a phase diagram finally led to the selection of a PLGA content of 70% (w/w) allowing to prepare stable NPs over a wide range of mannosylation (Figure 2A). Under these conditions, 100−200 nm NPs were obtained and exhibited a colloidal stability in water as well as in complex protein-containing dispersion media (Figure 2B). TEM analysis revealed the formation of spherical particles in the submicron range and overall confirmed the data obtained by dynamic light scattering (Figure 2C,D).

In order to develop formulations with tunable mannose surface densities, we varied the ratio of PLA-*b*-PEG-mannose to PLA-*b*-PEG from 0:100 to 100:0, resulting in the actual mannosylation of 0% to 65% of the PEG chain extremities, respectively (Table 1), due to the coupling yield of mannose in the synthesis of PLA-*b*-mannose. Neither hydrodynamic diameters nor zeta potentials were largely affected by the mannose content of the formulation (Table 1).

In order to characterize the core−shell structure of the prepared NP formulations (i.e., PEG chains and mannose residues on the outer surface), additional zeta-potential measurements in dependence on the pH of the dispersion medium were performed. With increasing amounts of mannose used in the NP formulation, a global shift toward higher zeta potential values was observed (Figure 3A). At pH 2, the zeta-potential of PLGA/PLA@PEG@mannose (100) NPs was 10 mV, while PLGA/PLA@PEG@mannose (50) was only slightly positive (3 mV) and PLGA/PLA@PEG even found to remain negative (−2 mV). One possible explanation for this observation is that the mannose component used for the polymer functionalization (*p*-aminophenyl-mannopryanoside) featured a secondary aromatic amine with a pK_a of about 4.5. At pH values below 4, a protonation of the amine groups occurs, leading to more positive zeta potential. Besides that, there might be also a global effect deriving from partial protonation of the PEG backbone itself, as can be seen from the increasing
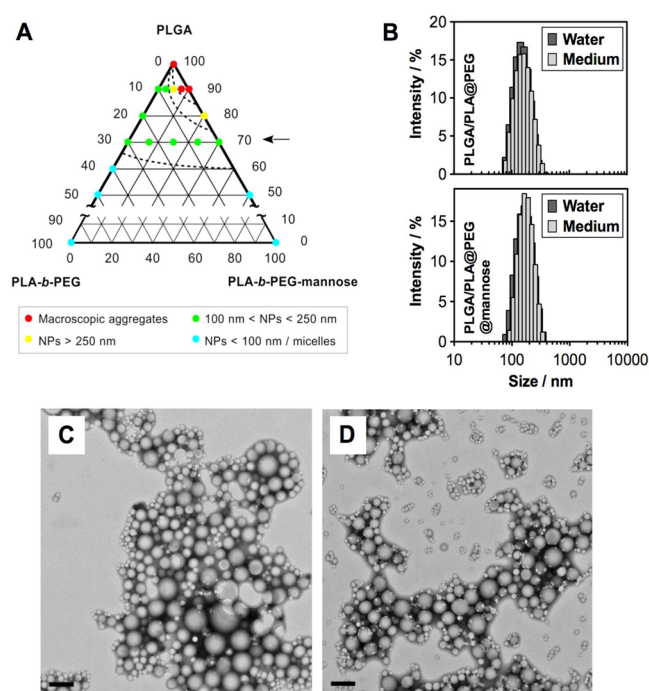
Figure 2. Formulation of mannosylated, PEGylated, polyester-based nanoparticles (PLGA/PLA@PEG@mannose). (A) Formation of colloidal suspensions of nanoparticles (NPs) from PLGA, PLA-*b*-PEG, and PLA-*b*-PEG-mannose copolymers, leading to the selection (arrow) of 70% PLGA-containing NPs and various PLA-*b*-PEG/PLA-*b*-PEG-mannose ratios, further characterized. (B) Comparison of intensity-based size distributions in water and RPMI (with 0.5% FCS) cell culture medium of PLGA/PLA@PEG (top) and PLGA/PLA@PEG@mannose NPs (bottom) as studied by dynamic light scattering. (C,D) Representative TEM images (20000× magnification) of PLGA/PLA@PEG (C) and PLGA/PLA@PEG@mannose (D). Scale bar: 200 nm.

zeta potential in the case of PLGA/PLA@PEG NPs. Nevertheless, these measurements confirmed the presence of mannose residues on the NP surface, and moreover, they can be used to indirectly monitor surface densities of the targeting ligand. Additional zeta potential measurements in dependence on ionic strength were carried out in order to determine the fixed aqueous layer thickness (FALT) as well as NMR measurements of PLA-*b*-PEG copolymers and PLGA/PLA@PEG NPs in different deuterated solvents, which confirmed the orientation of PEG on the outer surface facing the aqueous environment (Supporting Information Figure S2, Table S1).

In order to verify the biological activity of the mannose ligands on the surface of NPs, dynamic light scattering (DLS) was used to monitor the binding of the mannose-specific lectin concanavalin A (ConA) to the NP surface (Figure 3B). ConA is a tetrameric protein that has four binding sites specific for terminal nonreducing α-mannosyl residues.[34] It has been used to characterize the presence of sugars on the surface of colloidal carriers.[35] PLGA/PLA@PEG NPs (i.e., particles w/o mannose) did not show any change regarding their size distribution in the presence of ConA, indicating no interaction between the NP and the protein. However, the presence of mannose on the NP surface (PLGA/PLA@PEG@mannose (50) and (100), respectively) caused profound agglomeration when interaction with ConA was measured. The extent of agglomeration depended on the amount of mannose present on the NP surface, with more pronounced formation of agglomerates with
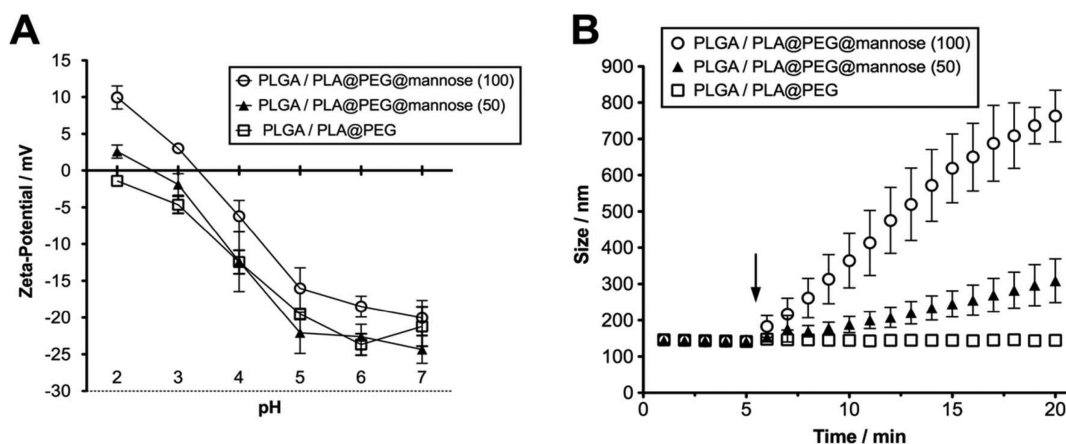
Figure 3. Characterization of NP surface mannosylation. (A) Zeta potential of PLGA/PLA@PEG@mannose NPs with different mannosylation ratios as a function of pH, detailing more positive values in the case of higher mannose−residue surface densities. (B) Concanavalin A-induced NP agglomeration in dependence on mannose−residue surface density, demonstrating the presence of biologically active mannose residues on the NP surface (see also Figure S3). The arrow depicts the time-point when Concanavalin A was added to the sample (2 μM final concentration). Data shown as mean ± SD ($n \geq 3$).
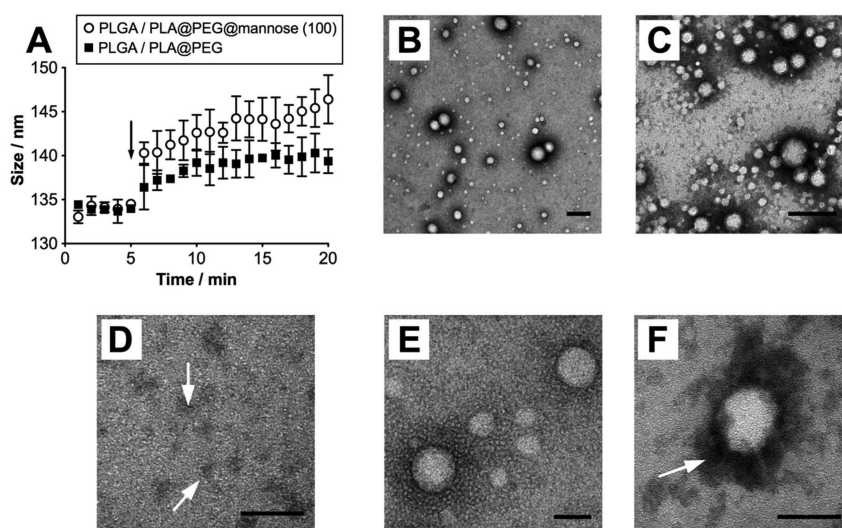

Figure 4. Interaction of SP-A with mannosylated NPs. (A) Binding of SP-A to PLGA/PLA@PEG and PLGA/PLA@PEG@mannose NPs, showing a more pronounced increase of the particle size over the time. The arrow indicates the addition of SP-A (20 μg·mL^{-1} final concentration). (B) Representative TEM images in negative staining of PLGA/PLA@PEG@mannose without SP-A (B,E), with SP-A (C,F), and SP-A alone (arrows, D), revealing stained protein associated with the NPs (arrow, F). Scale bar: 200 nm (B,C) or 50 nm (D−F). Data are shown as mean ± SD ($n = 3$).

the higher the content of PLA-*b*-PEG-mannose copolymer in the formulation. The minimum amount of PLA-*b*-PEG-mannose in the formulation necessary to induce agglomeration was found to be above 25% (w/w) since PLGA/PLA@PEG@mannose (25) NP did not agglomerate in the presence of ConA (Figure S3). ConA experiments confirmed that mannose molecules introduced by our technique at the surface of NPs are perfectly available to ConA and presented the right anomeric configuration to bind lectins such as SP-A.

Surfactant Protein A−Nanoparticle Interaction. The interaction between SP-A and NPs, containing or not mannose, was studied using DLS and TEM. SP-A bound to both types of formulations tested but showed a more pronounced increase of the particle size for PLGA/PLA@PEG@mannose NPs compared to mannose-free PLGA/PLA@PEG NPs (Figure 4A).

The average hydrodynamic diameter of both particle types studied in these experiments remained below 200 nm, and no formation of agglomerates could be observed. After addition of SP-A, the size of PLGA/PLA@PEG@mannose NPs increased by about 6 nm immediately, while mannose-free NPs only increased by less than 2 nm, indicating a more rapid onset of interaction in the case of mannosylated NP. Further, in the case of PLGA/PLA@PEG@mannose NPs, the average size difference after 20 min incubation was found to be approximately 14 nm, while the size of PLGA/PLA@PEG NPs increased by about 9 nm. The length of SP-A is between 16 to 19 nm, as described by Palaniyar et al.[36] We assume that by binding to surface-immobilized mannose residues via its carbohydrate recognition domain, SP-A forms a corona around the PLGA/PLA@PEG@mannose NPs. Possibly, the collagenous region of the protein is collapsed, what can be explained by the increase in size of about 7 to 8 nm regarding the thickness of the protein layer, suggesting a side onward binding of SP-A. Samples of both NP types with and without SP-A in the same ratio as studied by DLS were used for TEM analysis to visualize the
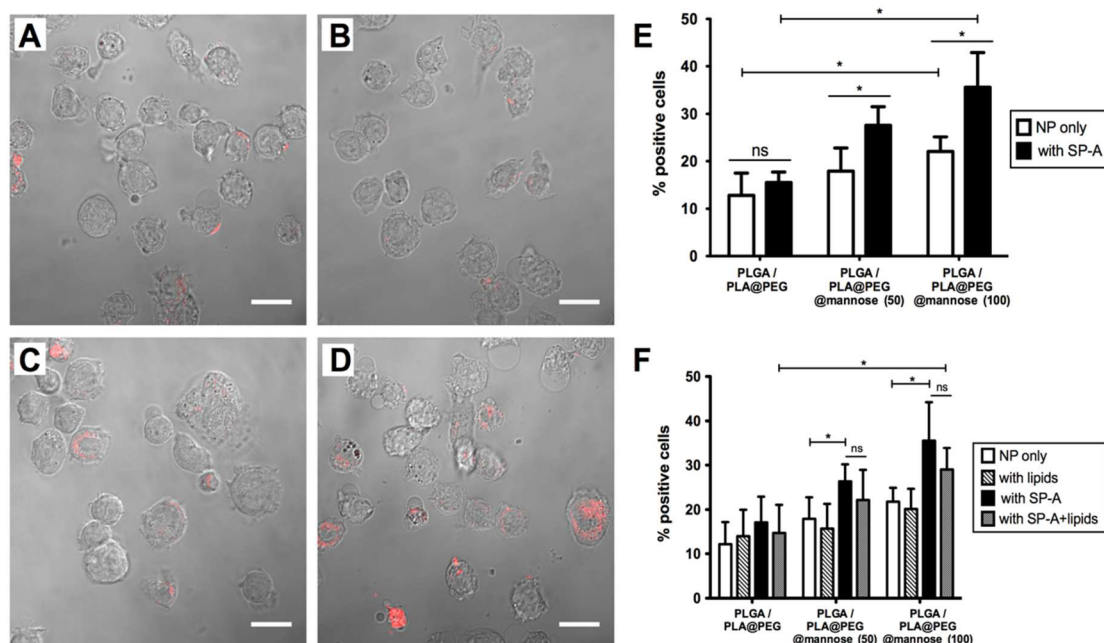
Figure 5. Influence of mannosylation and SP-A on nanoparticle interaction with macrophages. (A−D) Confocal micrographs (superimpositions of Nomarski and fluorescence images) showing the uptake of PLGA/PLA@PEG (A,B) and PLGA/PLA@PEG@mannose (100) NPs (C,D) by THP-1 monocyte-derived macrophages after 4 h in absence (A,C) or in the presence of SP-A (10 μg·mL^{-1}; B,D). (E) Flow cytometric quantification of cells positive for NP uptake in the presence and absence of SP-A (10 μg·mL^{-1}) after 4 h. Both methods reveal SP-A-mediated uptake by macrophages when mannose-residues are present on the NP surface. (F) Effect of surfactant-like lipids on SP-A mediated uptake of NPs, revealing a slight reduction in NP uptake in the presence of lipids (25 μg·mL^{-1}) as studied by flow cytometry. Data shown as mean ± SD (n = 6). The asterisk denotes a statistically significant difference ($p < 0.05$).

particles (Figure 4B−F) and the SP-A proteins using negative staining. Overall, micrographs of PLGA/PLA@PEG@mannose NPs revealed more dye associated in the presence of SP-A (Figure 4C,F), compared to absence of the protein (Figure 4B,E). Although dark spots associated with NP could also be observed in the absence of SP-A, the staining around NP displayed a much higher intensity for NP studied in the presence of SP-A. Additionally, in the case of the interaction of PLGA/PLA@PEG@mannose with SP-A, an unevenly shaped corona around the NP could be observed (Figure 4F).

Effect of SP-A on Nanoparticle Uptake by Macrophages. To study SP-A-mediated cellular interaction of the synthesized NP *in vitro*, we used THP-1 monocyte derived macrophages. Using confocal microscopy and flow cytometry, we tested whether NP−SP-A complexes are internalized by the macrophages and if SP-A can increase the cellular uptake of NPs. Confocal micrographs revealed that in the absence of SP-A, PLGA/PLA@PEG@mannose NPs showed a higher cellular interaction compared to PLGA/PLA@PEG NPs.

However, in the presence of SP-A, NP were associated and internalized with cells to a much higher extent (Figure 5A−D). PLGA/PLA@PEG@mannose NPs demonstrated the highest uptake when SP-A was present, while PLGA/PLA@PEG NPs showed neither in presence nor absence of SP-A any difference in uptake. Flow cytometry was used to quantify the previously observed effects (Figure 5E). NPs with mannose on the surface (i.e., PLGA/PLA@PEG@mannose (50) and (100), respectively) showed a higher uptake compared to PLGA/PLA@PEG NPs in the absence of SP-A. In the presence of SP-A, a significant increase in uptake of PLGA/PLA@PEG@mannose NPs was observed, while no difference could be detected in the case of PLGA/PLA@PEG NPs. The effect was found to be mannose concentration-dependent, whereas a loss of specificity

was observed at high protein concentrations (above 20 μg·mL^{-1}) (data not shown). The mechanism by which SP-A enhances endocytosis of mannose-containing nanoparticles might be (a) by direct binding of SP-A to mannose-containing NPs increasing SP-A/NP uptake by SP-A interactions with its receptors on macrophages;[13] and (b) by SP-A up-regulation of the mannose receptor (MR), a pattern recognition receptor expressed on AM.[36,37] Since pulmonary surfactant consists of about 90% lipid and 10% protein,[37] we also studied the effect of lipids on the NP uptake using an artificial lipid mix (DPPC/POPG/PA, 28:9:5.6 by weight) that is considered as the minimal essential lipids to mimic pulmonary surfactant studies.[26,38] The trend we observed was a reduction of the previously observed SP-A effects when lipids were added above a concentration of 25 μg·mL^{-1} (this reducing effect more pronounced at 100 μg·mL^{-1}; data not shown). These findings are in accordance with previous reports that showed that surfactant-like liposomes inhibited the SP-A-mediated increase in uptake of bacteria[39] or nanoparticles.[26]

Nanoparticle Uptake *in Vivo*. Using a microsprayer, aqueous NP suspensions (with and without SP-A) were administered intratracheally. After 4 h incubation, adherent cells (mainly AM) were isolated from broncho-alveolar lavages. Using flow cytometry, AM were then identified via surface marker labeling of CD11c in combination with autofluorescence, and fluorescent NP uptake was assessed in comparison to cells from untreated subjects.[31,40] PLGA/PLA@PEG NPs showed a high variance, but no difference in uptake regardless of the presence or absence of SP-A (Figure 6).

PLGA/PLA@PEG@mannose (100) NPs overall showed less variation, but a significant increase of particle uptake in the presence of SP-A. Thus, NPs with mannose on the surface sufficiently interacted with SP-A, leading to a higher uptake by
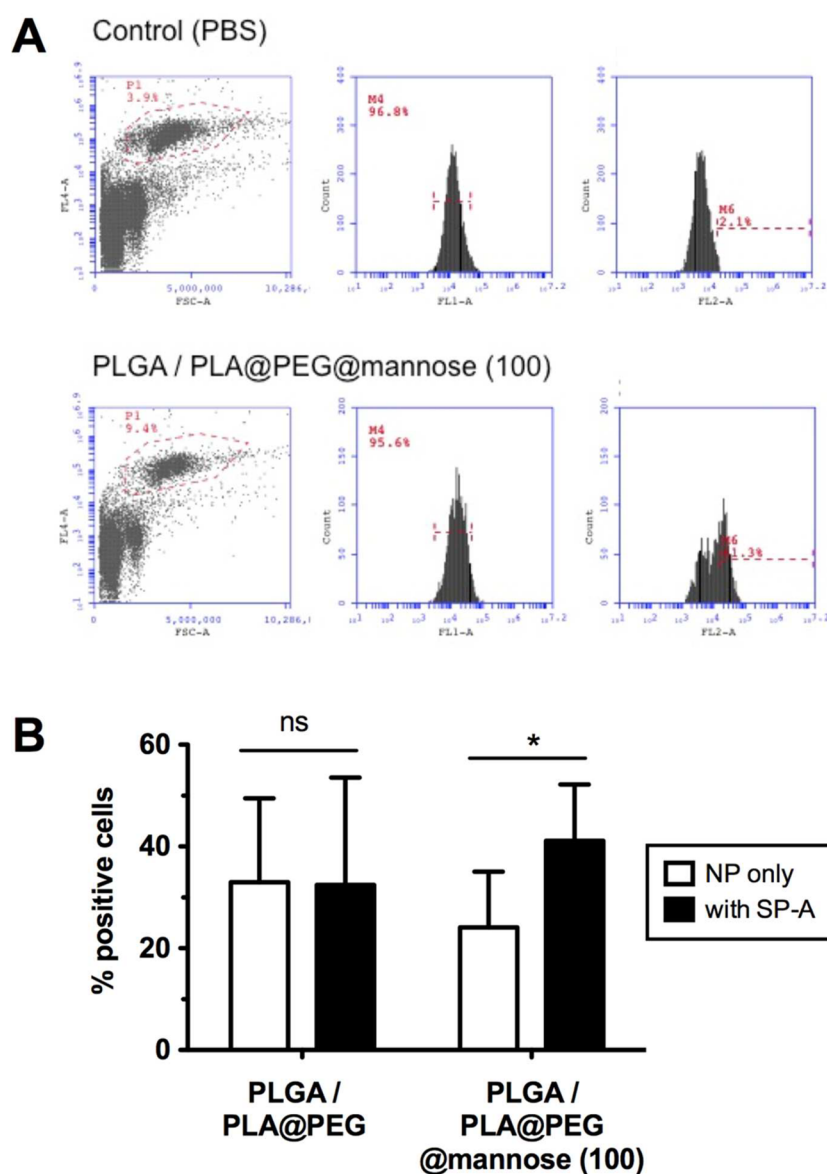
Figure 6. *In vivo* uptake of nanoparticles by alveolar macrophages following pulmonary administration to BALB/c mice. (A) Flow cytometric analysis of PLGA/PLA@PEG NPs, with and without mannose (Fl-2), in alveolar macrophages (CD 11c positive (Fl-4)), and high autofluorescence (Fl-1), applying a gating strategy described by Vermaelen et al.[31] As a control, untreated cells (PBS) were used. (B) NP uptake (with and without SP-A preincubation) in alveolar macrophages obtained from broncho-alveolar lavage 4 h after intratracheal instillation in BALB/c mice. Data shown as mean $\pm$ SD ($n = 6$). The asterisk denotes a statistically significant difference ($p < 0.05$).

AM. This increased uptake of mannosylated nanoparticle uptake in the presence of SP-A and the absence of effect of SP-A on the uptake of nonmannosylated nanoparticles are consistent with the *in vitro* data obtained with THP-1 macrophages (Figure 5E). *In vivo*, SP-A is described to be highly associated with lipids.[41] It is though that there are two pools of SP-A in the alveoli: lipid-bound SP-A and free protein. The majority of lipid-bound SP-A is concentrated in tubular myelin and large surfactant aggregates.[41] The lipid-free SP-A interacts with alveolar cells and is responsible for the effects of SP-A on the biology of AM. In the lung, changes in overall SP-A concentration as well as shifts in the ratio of free vs lipid-bound SP-A may alter the macrophage response to SP-A. We found here that in spite of the presence of surfactant lipids that cover macrophages and epithelial cells in the alveoli, SP-A significantly enhanced *in vivo* the uptake of NPs containing mannose, but only moderate NPs without mannose, by AM.

These findings are of interest since several studies have shown that the uptake of NPs by macrophages in the deep lungs is somehow poor.[39,42] Our results indicate that NPs decorated with mannose on their surface are efficient carriers to target AM *in vivo* as a consequence of both the presence of mannose on NP surface and the presence of SP-A in the alveolar fluid.

◼ CONCLUSION

In this article, we have shown that SP-A increases both *in vitro* and *in vivo* macrophage uptake of NPs containing mannose on their surface, allowing the controlled NP enrichment in AM. In future studies, drug-loaded NPs prepared from PLGA/PLA@PEG@mannose need to be evaluated regarding the capability of this system as a potential carrier system. PLA−PEG as the key composite of the here discussed delivery system is a well-characterized polymer that can be exploited both for the

entrapment of lipophilic and hydrophilic drug molecules.[43,44] The presented data, however, imply that this new approach might be very promising toward more specific treatments of infectious or inflammatory diseases in which the AM play a key role.

ASSOCIATED CONTENT

Ⓢ Supporting Information

The Supporting Information is available free of charge on the ACS Publications website at DOI: 10.1021/acs.molpharmaceut.6b00773.

> ^{1}H NMR, zeta potential, PEG layer thickness, Concanavalin A-induced NP agglomeration, and flow cytometric quantification (PDF)

AUTHOR INFORMATION

Corresponding Author

*Address: Institut Galien Paris-Sud, Faculté de Pharmacie, 5 rue JB Clément, 92296 Chatenay-Malabry Cedex, France. Tel: +33 1 46 83 55 68. Fax: +33 1 46 61 93 34. E-mail: elias.fattal@u-psud.fr.

ORCID Ⓘ

Julien Nicolas: 0000-0002-1597-0873

Notes

The authors declare no competing financial interest.

ACKNOWLEDGMENTS

REFERENCES

(1) Omlor, A. J.; Nguyen, J.; Bals, R.; Dinh, Q. T. Nanotechnology in respiratory medicine. *Respir. Res.* **2015**, *16*, 64.

(2) Ruge, C. A.; Kirch, J.; Lehr, C.-M. Pulmonary drug delivery: from generating aerosols to overcoming biological barriers—therapeutic possibilities and technological challenges. *Lancet Respir. Med.* **2013**, *1* (5), 402.

(3) Yu, M. K.; Park, J.; Jon, S. Targeting strategies for multifunctional nanoparticles in cancer imaging and therapy. *Theranostics* **2012**, *2* (1), 3−44.

(4) Mahon, E.; Salvati, A.; Baldelli Bombelli, F.; Lynch, I.; Dawson, K. A. Designing the nanoparticle−biomolecule interface for "targeting and therapeutic delivery. *J. Controlled Release* **2012**, *161*, 164.

(5) Fattal, E.; Grabowski, N.; Mura, S.; Vergnaud, J.; Tsapis, N.; Hillaireau, H. Lung toxicity of biodegradable nanoparticles. *J. Biomed. Nanotechnol.* **2014**, *10* (10), 2852−64.

(6) Grabowski, N.; Hillaireau, H.; Vergnaud, J.; Tsapis, N.; Pallardy, M.; Kerdine-Romer, S.; Fattal, E. Surface coating mediates the toxicity of polymeric nanoparticles towards human-like macrophages. *Int. J. Pharm.* **2015**, *482* (1−2), 75−83.

(7) Grabowski, N.; Hillaireau, H.; Vergnaud, J.; Santiago, L. A.; Kerdine-Romer, S.; Pallardy, M.; Tsapis, N.; Fattal, E. Toxicity of surface-modified PLGA nanoparticles toward lung alveolar epithelial cells. *Int. J. Pharm.* **2013**, *454* (2), 686−94.

(8) Aragao-Santiago, L.; Hillaireau, H.; Grabowski, N.; Mura, S.; Nascimento, T. L.; Dufort, S.; Coll, J. L.; Tsapis, N.; Fattal, E. Compared in vivo toxicity in mice of lung delivered biodegradable and non-biodegradable nanoparticles. *Nanotoxicology* **2016**, *10* (3), 292−302.

(9) Kishore, U.; Greenhough, T. J.; Waters, P.; Shrive, A. K.; Ghai, R.; Kamran, M. F.; Bernal, A. L.; Reid, K. B. M.; Madan, T.; Chakraborty, T. Surfactant proteins SP-A and SP-D: structure, function and receptors. *Mol. Immunol.* **2006**, *43* (9), 1293−1315.

(10) Lopez-Rodriguez, E.; Pérez-Gil, J. Structure-function relationships in pulmonary surfactant membranes: From biophysics to therapy. *Biochim. Biophys. Acta, Biomembr.* **2014**, *1838*, 1568.

(11) Haagsman, H. P. Interactions of surfactant protein A with pathogens. *Biochim. Biophys. Acta, Mol. Basis Dis.* **1998**, *1408* (2−3), 264−277.

(12) Tino, M. J.; Wright, J. R. Interactions of surfactant protein A with epithelial cells and phagocytes. *Biochim. Biophys. Acta, Mol. Basis Dis.* **1998**, *1408* (2−3), 241−263.

(13) Wright, J. R. Immunoregulatory functions of surfactant proteins. *Nat. Rev. Immunol.* **2005**, *5* (1), 58−68.

(14) Ernst, J. D. Macrophage receptors for Mycobacterium tuberculosis. *Infect. Immun.* **1998**, *66* (4), 1277−1281.

(15) Griffiths, G.; Nyström, B.; Sable, S. B.; Khuller, G. K. Nanobead-based interventions for the treatment and prevention of tuberculosis. *Nat. Rev. Microbiol.* **2010**, *8* (11), 827−834.

(16) Bhatt, K.; Salgame, P. Host innate immune response to Mycobacterium tuberculosis. *J. Clin. Immunol.* **2007**, *27* (4), 347−362.

(17) Russell, D. Mycobacterium Tuberculosis: Here Today, and Here Tomorrow. *Nat. Rev. Mol. Cell Biol.* **2001**, *2* (8), 569−586.

(18) Lawlor, C.; Kelly, C.; O'Leary, S.; O'Sullivan, M. P.; Gallagher, P. J.; Keane, J.; Cryan, S. A. Cellular targeting and trafficking of drug delivery systems for the prevention and treatment of MTb. *Tuberculosis* **2011**, *91* (1), 93−97.

(19) Diou, O.; Fattal, E.; Delplace, V.; Mackiewicz, N.; Nicolas, J.; Mériaux, S.; Valette, J.; Robic, C.; Tsapis, N. RGD decoration of PEGylated polyester nanocapsules of perfluorooctyl bromide for tumor imaging: Influence of pre or post-functionalization on capsule morphology. *Eur. J. Pharm. Biopharm.* **2013**, *87*, 170.

(20) Nijenhuis, A. J.; Grijpma, D. W.; Pennings, A. J. Lewis acid catalyzed polymerization of L-lactide. Kinetics and mechanism of the bulk polymerization. *Macromolecules* **1992**, *25* (24), 6419−6424.

(21) Jule, E.; Nagasaki, Y.; Kataoka, K. Lactose-installed poly-(ethylene glycol)-poly(d,l-lactide) block copolymer micelles exhibit fast-rate binding and high affinity toward a protein bed simulating a cell surface. A surface plasmon resonance study. *Bioconjugate Chem.* **2003**, *14* (1), 177−186.

(22) Beck-Broichsitter, M.; Rytting, E.; Lebhardt, T.; Wang, X.; Kissel, T. Preparation of nanoparticles by solvent displacement for drug delivery: A shift in the "ouzo region" upon drug loading. *Eur. J. Pharm. Sci.* **2010**, *41* (2), 244−253.

(23) Ruano, M. L.; García-Verdugo, I.; Miguel, E.; Pérez-Gil, J.; Casals, C. Self-aggregation of surfactant protein A. *Biochemistry* **2000**, *39* (21), 6529−6537.

(24) Sánchez-Barbero, F.; Rivas, G.; Steinhilber, W.; Casals, C. Structural and functional differences among human surfactant proteins SP-A1, SP-A2 and co-expressed SP-A1/SP-A2: role of supratrimeric oligomerization. *Biochem. J.* **2007**, *406* (3), 479−489.

(25) Sánchez-Barbero, F.; Strassner, J.; García-Cañero, R.; Steinhilber, W.; Casals, C. Role of the degree of oligomerization in the structure and function of human surfactant protein A. *J. Biol. Chem.* **2005**, *280* (9), 7659−7670.

(26) Ruge, C. A.; Schaefer, U. F.; Herrmann, J.; Kirch, J.; Cañadas, O.; Echaide, M.; Pérez-Gil, J.; Casals, C.; Müller, R.; Lehr, C.-M. The interplay of lung surfactant proteins and lipids assimilates the macrophage clearance of nanoparticles. *PLoS One* **2012**, *7* (7), e40775.

(27) Sáenz, A.; Cañadas, O.; Bagatolli, L. A.; Sánchez-Barbero, F.; Johnson, M. E.; Casals, C. Effect of surfactant protein A on the physical properties and surface activity of KL4-surfactant. *Biophys. J.* **2007**, *92* (2), 482−492.

(28) Grabowski, N.; Hillaireau, H.; Vergnaud-Gauduchon, J.; Nicolas, V.; Tsapis, N.; Kerdine-Romer, S.; Fattal, E. Surface-Modified Biodegradable Nanoparticles' Impact on Cytotoxicity and Inflamma-

tion Response on a Co-Culture of Lung Epithelial Cells and Human-Like Macrophages. *J. Biomed. Nanotechnol.* **2016**, *12* (1), 135−46.

(29) Segel, M. J.; Aqeilan, R.; Zilka, K.; Lorberboum-Galski, H.; Wallach-Dayan, S. B.; Conner, M. W.; Christensen, T. G.; Breuer, R. Effect of IL-2-Bax, a novel interleukin-2-receptor-targeted chimeric protein, on bleomycin lung injury. *Int. J. Exp. Pathol.* **2005**, *86* (5), 279−288.

(30) Maxeiner, J. H.; Karwot, R.; Hausding, M.; Sauer, K. A.; Scholtes, P.; Finotto, S. A method to enable the investigation of murine bronchial immune cells, their cytokines and mediators. *Nat. Protoc* **2007**, *2* (1), 105−12.

(31) Vermaelen, K.; Pauwels, R. Accurate and simple discrimination of mouse pulmonary dendritic cell and macrophage populations by flow cytometry: Methodology and new insights. *Cytometry* **2004**, *61A* (2), 170−177.

(32) Ruge, C. A.; Kirch, J.; Cañadas, O.; Schneider, M.; Pérez-Gil, J.; Schaefer, U. F.; Casals, C.; Lehr, C.-M. Uptake of nanoparticles by alveolar macrophages is triggered by surfactant protein A. *Nanomedicine* **2011**, *7* (6), 690−693.

(33) Nicolas, J.; Mura, S.; Brambilla, D.; Mackiewicz, N.; Couvreur, P. Design, functionalization strategies and biomedical applications of targeted biodegradable/biocompatible polymer-based nanocarriers for drug delivery. *Chem. Soc. Rev.* **2013**, *42* (3), 1147−1235.

(34) Goldstein, I. J.; Hayes, C. E. The Lectins: Carbohydrate-Binding Proteins of Plants and Animals*. In *Adv. Carbohydr. Chem. Biochem.*, Tipson, R. S., Derek, H., Eds. Academic Press: 1978; Vol. 35, pp 127−340.

(35) Muller, C. D.; Schuber, F. Neo-mannosylated liposomes: Synthesis and interaction with mouse Kupffer cells and resident peritoneal macrophages. *Biochim. Biophys. Acta, Biomembr.* **1989**, *986* (1), 97−105.

(36) Palaniyar, N.; Ridsdale, R. A.; Holterman, C. E.; Inchley, K.; Possmayer, F.; Harauz, G. Structural changes of surfactant protein A induced by cations reorient the protein on lipid bilayers. *J. Struct. Biol.* **1998**, *122* (3), 297−310.

(37) Blanco, O.; Pérez-Gil, J. Biochemical and pharmacological differences between preparations of exogenous natural surfactant used to treat Respiratory Distress Syndrome: role of the different components in an efficient pulmonary surfactant. *Eur. J. Pharmacol.* **2007**, *568* (1−3), 1−15.

(38) Sáenz, A.; Cañadas, O.; Bagatolli, L. A.; Johnson, M. E.; Casals, C. Physical Properties and Surface Activity of Surfactant-Like Membranes Containing the Cationic and Hydrophobic Peptide KL4. *FEBS J.* **2006**, *273* (11), 2515−2527.

(39) Geiser, M.; Casaulta, M.; Kupferschmid, B.; Schulz, H.; Semmler-Behnke, M.; Kreyling, W. The role of macrophages in the clearance of inhaled ultrafine titanium dioxide particles. *Am. J. Respir. Cell Mol. Biol.* **2008**, *38* (3), 371−6.

(40) Misharin, A. V.; Morales-Nebreda, L.; Mutlu, G. M.; Budinger, G. R. S.; Perlman, H. Flow Cytometric Analysis of Macrophages and Dendritic Cell Subsets in the Mouse Lung. *Am. J. Respir. Cell Mol. Biol.* **2013**, *49* (4), 503−510.

(41) Pérez-Gil, J. Structure of pulmonary surfactant membranes and films: the role of proteins and lipid-protein interactions. *Biochim. Biophys. Acta, Biomembr.* **2008**, *1778* (7−8), 1676−1695.

(42) Geiser, M. Update on macrophage clearance of inhaled micro- and nanoparticles. *J. Aerosol Med. Pulm. Drug Delivery* **2010**, *23* (4), 207−217.

(43) Govender, T.; Riley, T.; Ehtezazi, T.; Garnett, M. C.; Stolnik, S.; Illum, L.; Davis, S. S. Defining the drug incorporation properties of PLA-PEG nanoparticles. *Int. J. Pharm.* **2000**, *199* (1), 95−110.

(44) Riley, T.; Stolnik, S.; Heald, C. R.; Xiong, C. D.; Garnett, M. C. Physicochemical Evaluation of Nanoparticles Assembled from Poly-(lactic acid)−Poly(ethylene glycol) (PLA−PEG) Block Copolymers as Drug Delivery Vehicles. *Langmuir* **2001**, *17* (11), 3168−3174.